3D Visualization of Radar Coverage Considering Electromagnetic Interference

HANG QIU[1,2,3] LEI-TING CHEN[1,3] GUO-PING QIU[2] CHUAN ZHOU[1,2,3]
[1] School of Computer Science & Engineering, University of Electronic Science and Technology of China, Chengdu, CHINA
[2] School of Computer Science, University of Nottingham, Nottingham, UNITED KINGDOM
[3] Provincial Key Laboratory of Digital Meida, Chengdu, CHINA
qiuhang@uestc.edu.cn

Abstract: -Radar plays an important role in many domains, such as target searching, target tracking and dynamic objects detection. However, the electromagnetic information of radar is invisible and full of changes in real time, which restricts users to plan and design the radar systems. In recent years, with the development of interactive visualization technology, 3D visualization of the abstract information of radar coverage under the influence of complicated environment becomes a hotspot. In this paper, we present a method to represent radar coverage considering the electromagnetic interference. Based on the radar equation, from the perspectives of pitch and azimuth angles to achieve 3D modeling of radar coverage through discrete subdivision, and the radar model possesses self-adaptability to different levels of detail. The 3D radar detection range under the influence of electromagnetic interference is analyzed and addressed based on radar jamming model. Experiments demonstrate that our method not only can efficiently complete the three-dimensional modeling of radar, but also visually show the true radar coverage under the influence of complex electromagnetic environment.

Key-Words: - 3D visualization, radar coverage, levels of detail (LOD), electromagnetic interference, non-uniform sampling

1 Introduction

Radar bears great application values in civil and military fields such as meteorological detection, ocean waves measuring, air traffic control, and so on. Radar uses electromagnetic waves to identify range, altitude, direction, or speed of both moving and fixed objects, including airplanes, ships, clouds, and invisible obstacles. A radar system has a transmitter that emits microwaves or radio waves, which are emitted in certain phase and frequency. When the waves hit an object, they are scattered in all directions and partly reflected back with a slight change of wavelength if the target is moving. The received signals can be amplified in the antenna configuration and then in the receiver to detect objects at distance.

Radar's electromagnetic information is invisible and full of changes in real time. The traditional 2D radar coverage diagrams drawn by hand or aimed by computers have some evident shortages: 2D curve cannot intuitively represent radar electromagnetic information; 2D radar coverage diagrams cannot represent the effects of jamming coming from different directions or distance.

In recent years, extensive works [1-4] made efforts to express the radar electromagnetic information in three-dimensions. Based on different theories and application purposes, the 3D visualization methods for radar coverage can roughly be classified into three following categories.

(1) Radar Equation-based Method

The principle of this method includes two steps: firstly, the radar's coverage is calculated by employing the radar equation. Secondly, according to the specific factors those affect the radar coverage, such as terrain occlusion, electromagnetic interference and atmospheric effects, the model boundary points are revised to achieve 3D visualization of coverage under different circumstances.

Based on radar equation, Zhang et al. [5] implemented the 3D visualization of the search radar by using Matlab and C program. Lin et al. [6] adopt radar equation to calculate vertex coordinates of lobe, and construct 3D representation of radar detection range.

Above-mentioned researches confine the radar electromagnetic environment to pure free space, which has no regard to other factors such as terrain occlusion and atmospheric effects. Kostic et al. [7] and Rancic et al. [8] considered theses environmental influences and realized the 3D

display of radar coverage by overlapping 2D detection graph. Meng [9] applied radar equation to represent 3D radar model in free space and implemented the influence of atmosphere and terrain by revising the boundary vertices of the radar model. Based on this method, [10] presented novel revised algorithm under terrain occlusion. Chen et al. [11] proposed beam-drawing methods in spatial domain, and presented corresponding model revised algorithm considering the influence of terrain. Most recently, Yang et al. [12] and Li et al. [13] designed and realized the representation of 3D electromagnetic situation for military applications.

(2) Parabolic Equation-based Method

The parabolic equation-based method estimates the pattern propagation factor by parabolic equation first, and then calculates the radar coverage by radar equation. Nevertheless, parabolic equation-based method has high computation complexity and it is not based on actual electromotive parameters.

Awadallah et al. [14] applied parabolic equation to research radar-propagation-model in three-dimension space. Yang et al. [15] considered the effect of most real environment factors with parabolic equation, and visualized the 3D radar maximum detection range.

(3) Advanced Propagation Model-based Method

In advanced propagation model-based method, different computational models are employed with different electromagnetism regions according to the propagation attenuation computational models. Although this method is faster than parabolic equation-based method, it is very time consuming and has relatively high demand on model precision.

Based on advanced propagation model, [16, 17] discussed the radar 3D visualization approaches in complicated environment. Chen et al. [18] put forward GPU-based hardware-accelerated algorithm to handle with the limited rendering speed. Zhang et al. [19] described the algorithm for 3D visualization of radar detection range based on revised advanced propagation model.

In this paper, we present a method for 3D visualization of radar coverage under the influence of electromagnetic interference based on radar equation. We focus on simulating the essential behaviours of radar and looking for the right compromise between realism and efficiency.

The rest of the paper is organized as follows. Section 2 briefly depicts the radar-jamming model. Section 3 discusses the hybrid sampling-based radar 3D modeling method in free space. Section 4 focuses on the specific implementation approach. Section 5 gives the acceleration strategy for 3D visualization of radar. Section 6 presents experiments to illuminate the performance of our method. The conclusion of this paper is given in Section 7.

2 The Model of Radar Jamming

The radar that detects in a fixed direction with specific pitch (θ) and azimuth (φ) angles is determined by Equation (1):

$$R(\theta,\varphi)=\left[\frac{P_t G_t G_r \sigma \lambda^2 F_t^2 F_r^2}{(4\pi)^3 P_r}\right]^{1/4} \quad (1)$$

where $R(\theta, \varphi)$ is the distance between radar source and the target with specified pitch and azimuth angles. P_r is the receiving terminal power. P_t is the transmitter power. G_t is the transmitting antenna power gain. G_r depicts the receiving antenna power gain. σ is the radar target's cross section. λ is wavelength. F_t is pattern propagation factor from transmitting antenna to the target, and F_r is pattern propagation factor from target to the receiving antenna.

Pattern propagation factors F_r and F_t are space coordinates-related variables, which are functions of the space-vector (θ, φ). We only need to consider variables in this part and simplify the calculation. Therefore, Equation (1) can be rewritten as

$$R(\theta,\varphi)=R_{\max}\times\sqrt{F_r(\theta,\varphi)\times F_t(\theta,\varphi)} \quad (2)$$

where $R_{\max}$ is the radar's maximum radiation range in free space when F_r and F_t are at the maximum, which equals to 1. The existing radar's transmitting and receiving antennas are often the same antenna. So we can further set $F_r = F_t$. Then, the final equation of radar range calculation is:

$$R = R_{\max}\times F(\theta,\varphi) \quad (3)$$

In free space, radar electromagnetic waves transmit in the form of spherical surfaces. The outer surface is determined by the range equation above with varying pitch and azimuth angles.

Radar can be affected by a variety of electromagnetic interferences, such as stand-off jamming, random jamming, self-defense jamming and so on. In this paper, we focus on stand-off jamming. As shown in Fig. 1, assume that the jammer and radar are in stationary state and the target is a dynamic object. The angle between

jamming signal and the direction of radar antenna is α.

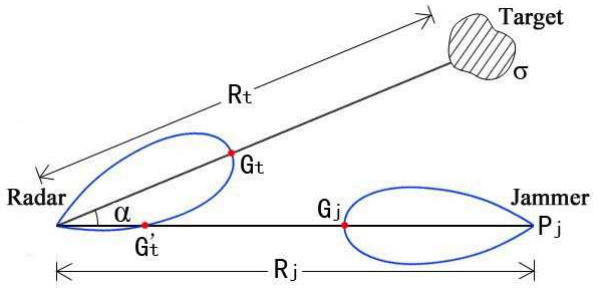

Fig. 1 The principle of stand-off jamming

In general, when radar detects or tracks a target, the main lobe of radar points to the target. At the same time, in order to protect the target, the antenna of jammer points to radar, which plays the role of suppression. Therefore, there are two signals received by the radar receiver, i.e. response signal P_{rs} from target and jamming signal P_{rj} from the jammer.

Based on the radar equation, P_{rs} can be expressed as:

$$P_{rs} = \frac{P_t G_t^2 \sigma \lambda^2}{(4\pi)^3 R_t^4} \tag{4}$$

P_t is the radar transmitted power. G_t is the antenna gain. σ depicts radar cross section. R_t is the distance between radar and the target.

The jamming signal P_{rj} can be calculated as:

$$P_{rj} = \frac{P_j G_j G_t^{'} \lambda^2 \gamma_j}{(4\pi)^2 R_j^2} \tag{5}$$

P_j is the transmitted power of the jammer. G_j is the antenna gain. R_j depicts the distance between jammer and radar. γ_j is the polarization coefficient. $G_t^{'}$ is the radar antenna gain in the direction of the jammer.

According to the different performance of radar, when the value of jamming signal is far less than the value of response signal, the jamming signal can be automatically filtered. However, when response signal conforms to a certain relationship with jamming signal, the receiver cannot differentiate these two signals, which leads to the deviation of radar detection.

To measure the performance of the jamming effect and the anti-jamming capability, power criterion is usually applied, which depicts the power relationship between response signal and jamming signal in effective jamming situation. K_j is suppression coefficient that can be expressed as follows:

$$K_j = P_j / P_s \tag{6}$$

The value of suppression coefficient depends on the jamming signal's modulation and the type of radar. The smaller the suppression coefficient is, the worse the anti-jamming capability is.

For particular radar and jammer, the suppression coefficient is fixed. According to Equation (4), Equation (5) and Equation (6), the radar jamming equation can be expressed as follows:

$$\frac{P_{rj}}{P_{rs}} = \frac{P_j G_j}{P_t G_t} \times \frac{4\pi \gamma_j}{\sigma} \times \frac{G_t^{'}}{G_t} \times \frac{R_t^4}{R_j^2} \geq K_j \tag{7}$$

When the power ratio is greater than suppression coefficient, the effective jamming is generated. The space that satisfies jamming equation is called suppressing zone. To calculate the effective detection range of radar under the situation of jamming and visualize the boundary of radar sampling points, we set the value of P_{rj}/P_{rs} equals to suppression coefficient K_j. Thus, the effective detection range of radar can be calculated as:

$$R_0^4 = \frac{K_j P_t G_t^2 \sigma R_j^2}{4\pi \gamma_j P_j G_j G_t'} \tag{8}$$

G_t' is a variable, which related to the angle α between jamming signal and radar antenna, as shown in Fig. 1. According to the empirical formula of antenna gain, $G_t'(\alpha)$ can be expressed as:

$$\begin{cases} G_t'(\alpha) = G_t & 0 \leq \alpha \leq \theta_{0.5}/2 \\ G_t'(\alpha) = k\left(\dfrac{\theta_{0.5}}{\alpha}\right)^2 G_t & \theta_{0.5}/2 \leq \alpha \leq 90^\circ \\ G_t'(\alpha) = k\left(\dfrac{\theta_{0.5}}{90}\right)^2 G_t & \alpha \geq 90^\circ \end{cases} \tag{9}$$

According to the different values of α, the curve of radar detection range can be achieved, as shown in Fig. 2.

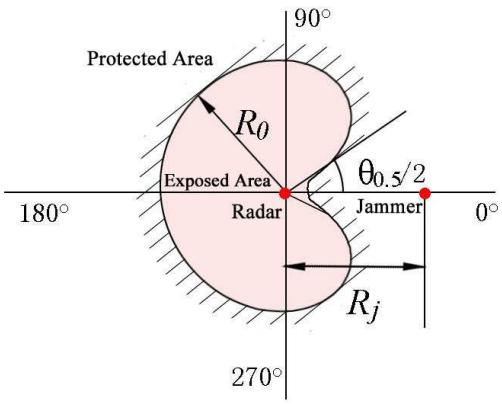

Fig. 2 Schematic diagram of protected area

The curve defines the effective radar detection range and the jamming range of jammer. When the target moves into the shadow area ($P_{rj}/P_{rs} < K_j$), the jamming signal cannot suppress the response signal, and the target can be detected by radar. This area is called *exposed area*.

When the target leaves exposed area ($P_{rj}/P_{rs} > K_j$), the jamming signal can suppress the response signal, and the target cannot be detected by radar. This area is called *protected area*.

When $P_{rj}/P_{rs} = K_j$, R_0 is the boundary between protected area and exposed area. From the viewpoint of jammer, R_0 is the minimum jamming distance, which usually called *exposed radius*.

When multiple jamming sources exist, the suppression of jammer in one particular direction can be equivalent to numeral superposition of all the jammers' suppressions in this direction. Thus, the jamming equation for multiple jamming sources can be expressed as follows:

$$\sum_{k=1}^{n}\frac{P_{r,k,j}}{P_{r,s}}=\sum_{k=1}^{n}\left(\frac{P_{k,j}G_{k,j}\gamma_{i,j}}{P_tG_t\sigma}\cdot\frac{4\pi R_t^4}{R_{k,j}^2}\cdot\frac{G'_{k,t}}{G_t}\right)\geq K_j \quad (10)$$

The boundary of exposed area can be calculated as:

$$R_t^4=K_j\Big/\sum_{k=1}^{n}\left(\frac{P_{k,j}G_{k,j}\gamma_{k,j}}{P_tG_t\sigma}\cdot\frac{4\pi}{R_{k,j}^2}\cdot\frac{G'_{k,t}}{G_t}\right) \quad (11)$$

$G'_{k,t}$ is a variable, which related to the angle α_n between n*th* jamming signal and radar antenna. $G'_n(\alpha_n)$ can be depicted as:

$$\begin{cases} G'_{n,t}(\alpha)=G_t & 0\leq\alpha\leq\theta_{0.5}/2 \\ G'_{n,t}(\alpha)=k\left(\dfrac{\theta_{0.5}}{\alpha}\right)^2G_t & \theta_{0.5}/2\leq\alpha\leq 90^\circ \\ G'_{n,t}(\alpha)=k\left(\dfrac{\theta_{0.5}}{90}\right)^2G_t & \alpha\geq 90^\circ \end{cases} \quad (12)$$

3 Hybrid Sampling-based Radar 3D Modeling in Free Space

To visualize the radar coverage under the influence of electromagnetic interference, we apply radar equation-based method. Firstly, we consider the 3D modeling of radar coverage in free space. Secondly, according to the model of radar jamming, we revise the 3D model boundary points to achieve the visualization of radar coverage under the influence of electromagnetic interference. In this section, we give details of 3D modeling of radar coverage in free space.

As mentioned in Section 2, radar electromagnetic waves transmit in the form of spherical surfaces in free space. The outer surface is determined by the range equation expressed by Equation (3) with varying pitch and azimuth angles. Therefore, based on the idea of discrete sampling and approximation, the outer boundary surface can be sampled by using the radar range equation. Each discrete vector (θ, φ) and the detection range $R(\theta,\varphi)$ together forms a 3D point $P(\theta, \varphi, R)$. The discrete boundary points constitute the necessary grid for drawing the corresponding radar coverage for 3D visualization.

As shown in Fig. 3, the radar electromagnetic waves form an outer surface centred at the radar transmitter/receiver, where θ and φ correspond to the radar's pitch and azimuth angles respectively.

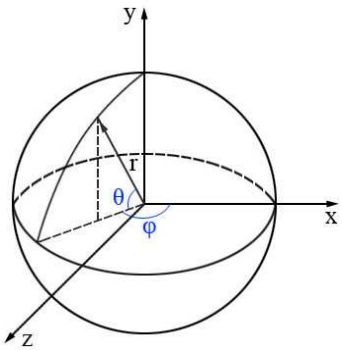

Fig. 3 Schematic diagram of the radar spherical coordinate system

Assuming the radar model is scanning omni-directional, the pitch angle is in the range of [-90°,

90°] and the azimuth angle is a circle in the range of [0°, 360°]. We dissect the whole sphere in pitch and azimuth directions.

***Azimuth dissection*:** perpendicular to the plane of azimuth, the sphere is split into n slices α_n. Each slice corresponds to a azimuth angle φ_n.

***Pitch dissection*:** starting from the centre of the radar, m vectors are range-calculated corresponding to a unique pitch angle θ_m.

The issue boils down to how to determine the angle sampling steps. Uniform sampling is a natural choice, as shown in Fig. 4.

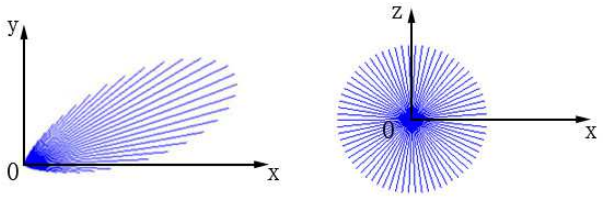

(a) Pitch angle sampling (b) Azimuth angle sampling

Fig. 4 The uniform sampling method

Uniform sampling is easy to implement. However, some feature points on the radar beams may be lost between the sampling steps. Meanwhile, there are also many points whose detection range is 0, which lead to unnecessary calculation. In this paper, we present a hybrid sampling method: in the pitch direction, sampling is separated into sub-regions respectively based on the characteristics of the radar beams; in the azimuth direction, sampling is in accordance with terrain resolution, as discussed in detail below.

3.1 Azimuth Sampling

In the azimuth direction, sampling step length is determined by the terrain revolution, as shown in Fig. 5.

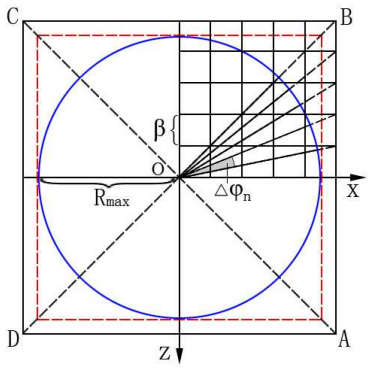

Fig. 5 Determine azimuth sampling step length

The procedure includes two steps:

Step 1. Pre-computing of step length: The radar's centre O is initialized at some intersection of the terrain grid. The horizontal axis of the radar's coordinates coincides with one of the terrain grid lines. The detection range of the radar's maximum radiation direction $R_{\max}$ is taken as a radius to form a circle, which is used to obtain the minimum square-shaped terrain grid ABCD that completely covers the circle. The terrain is divided into $n \times n$ grids with the resolution of β. Then, connecting the centre and the square's border grids forms the intersection points and the azimuth sampling steps. The angle $\Delta\varphi_n$ between the adjacent connected lines is the actual azimuth sampling step length. No matter whether the peripheral grid is tangential to the circle or not, the angle divisions are symmetric along horizontal and vertical directions. Therefore, we only need to pre-compute 1/8 of the sampling directions.

Step 2. Azimuth dissection: the pre-computed sampling step lengths $\Delta\varphi_n$ are used to accomplish discrete dissection. The number of dissections is expressed as variable *Pieces*, which will be used in the data structure discussed in following section.

The above-mentioned method implements one-to-one correspondence between the radar's azimuth sampling and the terrain grid, which improves self-adaptability of the radar model to different terrain resolutions.

When discretization is completed, the continuous spherical shell is divided into a number of vectors. The vector $R(\theta_i, \varphi_j)$, or simply $R_{i,j}$, corresponds to the radar detection range, which determines a boundary point $P(\theta_i, \varphi_j, R_{i,j})$. Substituting each direction's corresponding vector $R(\theta_i, \varphi_j)$ into Equation (3), we can obtain the maximum detection range corresponding to the vector.

As shown in Fig. 6, considering the extreme case, i. e. the radius of radar is smaller than the distance of adjacent terrain sampling points, we still can use 8 points to represent the radar detection range.

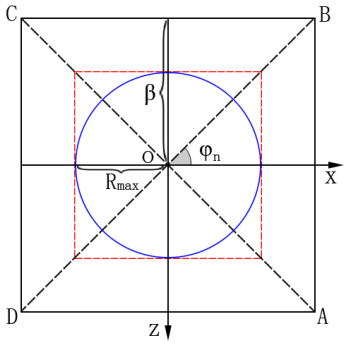

Fig. 6 Azimuth angle sampling in special circumstance

3.2 Pitch Sampling

Most of the radar coverage information is concentrated within the half-power lobe, i.e. between two 3dB attenuation points, as shown in Fig. 7.

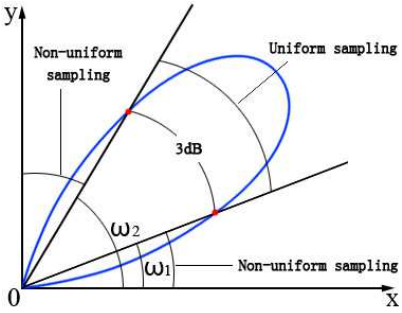

Fig. 7 Sub-regional sampling in pitch angle

Beyond this zone, there are many points with detection ranges close to 0. Therefore, we apply 3dB attenuation points as boarder markers to divide radar coverage into three distinct areas in pitch direction, and sample them separately using two different methods.

The radar half-power beamwidth is defined as the degree of angle between the two 3dB attenuation points from the origin, by which two 3dB attenuation points at pitch angles ω_1 and ω_2 can be determined. As shown in Fig. 6, the farther away the range directions are from the boundary lines through the two 3dB attenuation points, the closer the range detections are towards 0, thus fewer samplings are needed. Therefore, uniform sampling is employed within interval $[\omega_1, \omega_2]$ to guarantee that the main feature, shape, and resolution of the radar detection information are acquired. In the interval $[0, \omega_1)$ and $(\omega_2, 90°]$, sampling steps are automatically augmented according to the angle away from the boundary lines to the horizontal or vertical axis. The specific sampling methods are as follows:

$$\theta_{i+1} = \begin{cases} \theta_i + (|\theta_i - \theta_0|)/m & \theta_i \geq \omega_2, \theta_i < \omega_1 \\ \theta_i + elevation\_step & \omega_1 \leq \theta_i < \omega_2 \end{cases} \quad (13)$$

where $|\theta_i - \theta_0|$ is the difference between the pitch angle and the initial elevation angle. $elevation\_step$ is the step length when fully uniform sampling is employed. m is the proportional coefficient, which determines variation of sampling step length. The number of sampling in pitch angle direction is indicated as variable *Layers*. Equation (13) is used to automatically calculate corresponding actual number of sampling points. The procedure includes three steps:

Step 1. Calculation of *elevation_step*

We apply the proportional relationship between sampling step length and curvature radius to convert the sampling step length in azimuth angle to *elevation_step*.

The curvature radius of curve in azimuth angle is $R_{\max}$. The curvature radius of curve in pitch angle is changing. As shown in Fig. 8, we use the two 3dB attenuation points B, C and the boundary point of initial pitch angle to calculate the corresponding curvature radius *R_elevation*.

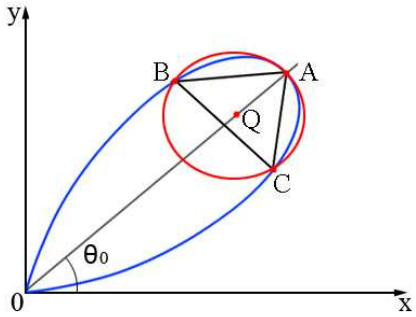

Fig. 8 Calculation of curvature radius

The smaller the curvature radius is, the smaller the sampling step length is. Thus, the relationship between curvature radius and sampling step length in azimuth and pitch angle can be expressed as:

$$\frac{elevation\_step}{az\_step} = k \cdot \frac{R\_elevation}{R_{\max}} \quad (14)$$

Step 2. Calculation proportional coefficient *m*

The value of m affects the number of sampling points and its value depends on $elevation\_step$. According to piecewise function, in order to achieve smooth transition between uniform sampling zone and non-uniform sampling zone, the sampling step length must be continuous in piecewise function. Assume that the 3dB attenuation point ω_1 is the piecewise point of piecewise continuous function. Thus, the m can be calculated as:

$$m = \frac{\theta_0 - \omega_1}{elevation\_step} \quad (15)$$

Step 3. Pitch dissection

Put the value of $elevation\_step$ and m into Equation (13), sampling step length can be achieved.

4 The Rendering of Radar

4.1 Discrete-side Rendering

As mentioned in Section 2, we dissect the whole sphere in pitch and azimuth direction. Thus, we

apply an array $FixBound[Layers][Pieces]$ to store each sampling point's coordinates in the radar coordinates system, which is calculated as:

$$\begin{cases} FixBound[i][j].x = R\_\max[i][j] \times \cos\theta\cos\varphi \\ FixBound[i][j].y = R\_\max[i][j] \times \sin\theta \\ FixBound[i][j].z = R\_\max[i][j] \times \cos\theta\sin\varphi \end{cases} \quad (16)$$

Here we redefine an array $Bound[Layers][Pieces]$ to store each discrete point's coordinates in the world coordinates system as follows to improve the efficiency:

$$\begin{cases} FixBound[i][j].x = FixBound[i][j] + position\_x \\ FixBound[i][j].y = FixBound[i][j] + position\_y \\ FixBound[i][j].z = FixBound[i][j] + position\_z \end{cases} \quad (17)$$

When the radar system is moving in the virtual scene, the center or origin changes, but the coordinates of boundary sampling points remain the same, which are stored in the array *FixBound* beforehand. Accordingly, we only need to adjust *Bound* to renew the coordinates of boundary points in the world coordinates system.

When the discrete boundary points are obtained, the discrete grid vertices can be calculated. In the azimuth direction, the points are connected to form a coil according to their positions in the space, as shown in Fig. 9 (a). In the pitch direction, the points are connected to form a beam ring, as shown in Fig. 9 (b). Finally, we get a gridded radar coverage mesh, as shown in Fig. 9 (c).

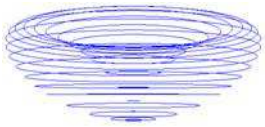

(a) Azimuth angle sampling

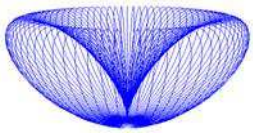

(b) Pitch angle sampling

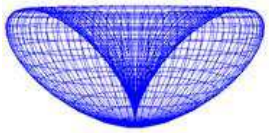

(C) Spatial drawing effect

Fig. 9 Radar coverage mesh as discrete vertices

4.2 Implementation of Jamming Effect

We use coil in the azimuth direction as the basic processing unit and apply jamming equation to calculate the position of each sampling points in real time. In each frame, we revise the points to the exact position in the curve boundary as shown in Fig. 2, and connect the discrete points to construct mesh. To improve clarity, let us take an example. Assume $\theta_{0.5}/2 < \alpha < 90^\circ$, the specific steps are as follows.

Step 1. Invariant pre-computation

Equation (8) can be rewritten to Equation (18) when all the parameters of radar and jammer are known.

$$R_0^2 = \frac{R_j \alpha}{\sqrt{C}} \quad (18)$$

Where $C = \dfrac{P_j G_j \gamma_j 4\pi K \theta_{0.5}^2}{P_t G_t K_j \sigma}$. C is a invariant, which related to the parameters of radar, target and jammer.

Step 2. Sampling points revision in pitch direction

According to the pitch dissection, different pitch angle corresponds to different Azimuth coil. The sampling points in a coil have the same pitch angle. We can use Equation (16) to calculate detection range directly. All the sampling points in Azimuth coils are calculated in sequence, and the final radar detection boundary is achieved.

Step 3. Mesh construction of discrete points

Connect the sampling points in pitch and azimuth direction and construct 3D mesh.

5 LOD-based Acceleration Strategy

To show the details of the radar coverage, a single radar model needs numerous points to express. When the viewpoint is far away from the model, the employment of high-resolution model description is unnecessary. Our consideration is to make the model's resolution adjusts automatically according to the viewpoint orientations.

Our view-dependent model approach is as follows. The distance between the viewpoint and the radar's center is collected in real-time, which is used to decide the model's levels of detail. Blending is used for switching between levels of detail to achieve smooth transition, as shown in Fig. 10.

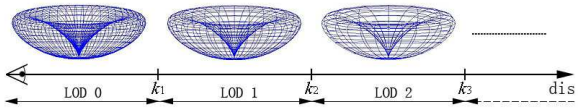

Fig. 10 View-dependent level of detail

When the distance between viewpoint and radar centre is $(0 \sim k_1)$, the level $l = 0$, and the original model resolution is rendered. When the distance is $(k_1 \sim k_2)$, the level $l = 1$, and the simplified model is rendered. When the distance is $(k_2 \sim k_3)$, the level

$l=2$, the simplified model based on level 1 is rendered and so on.

Assume that the current level is l, and the direction of azimuth angle begins with 0. The points numbered $m=2^l\times i$ (i is positive integer, and $m \le Pieces$) are needed to render and the rendering step in azimuth angle is 2^l.

(1) $l=0$, all the points are rendered, as shown in Fig.11 (a).

(2) $l=1$, it skips sampling points, as shown in Fig. 11 (b).

(3) $l=2$, it further skips sampling points based on medium resolution model, as shown in Fig. 11 (c).

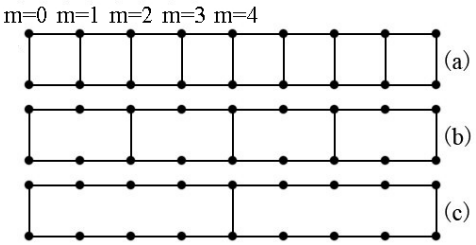

Fig. 11 Model with multiple levels of detail

Theoretically, the procedures described above are endless. We set a threshold to avoid the unlimited simplification of model.

The discrete levels of detail may make the transition visible. To avoid popping artifacts appearing, seamless transition scheme is indispensable.

Assume that the distance between viewpoint and radar is dis, the whole area is divided into n levels by the boundary points k_0, k_1, k_2, k_3, ……, k_n. We accomplish smooth transition by establishing a transition zone between each adjacent levels. Transparency of the vertices and lines in the transition zone changes with distance.

For level l, in the transition zone, the points numbered $2^{l+1}\times i$ are needed to be rendered in level $l+1$ and the alpha values of these points are set 1. The points numbered $2^l(2i+1)$ will be simplified in level $l+1$ and the corresponding alpha values can be calculated as:

$$fade = 1-\frac{dis-k_l}{k_{l+1}-k_l} \qquad (19)$$

Where $dis-k_l$ depicts the distance between model and the transition zone. $k_{l+1}-k_l$ is the length of the transition zone.

6 Experiments and Discussions

We use OpenGL on C++ platform to implement the method presented in this paper, and carry out related experiments on PC. The computer configuration used for experiments is Windows XP operating system, Intel Pentium 3.4 GHz CPU, 1G memory, and ATI FireGLV3100 graphics card.

In the experiments, we select Gaussian pattern function commonly used in the radar equation: $F=e^{-k\theta^2}$ ($k=4\ln\sqrt{2}\theta_b^2$, where θ_b is the beamwidth). The parameters of radar and jammer are shown in Table 1 and Table 2 respectively.

Table 1. Radar Parameters

Parameter Name	Values
Transmitted power	4000kw
Frequency	3000MHz
Antenna gain	40dB
Antenna side lobe gain	-10dBi
Pulse repetition frequency	250HZ
System loss	12dB
Probability of detection	0.9
Probability of false alarm	10^{-6}
Vertical beam width	30°
Elevation	30°
Antenna speed	36°/s

Table 2. Jammer Parameters

Parameter Name	Values
Transmitted power	2000kw
Initial distance	185km
Antenna gain	5dB
System loss	7dB
Polarization coefficient	1
Suppression coefficient	2

To testify the advantage of radar modeling based on our hybrid sampling, we carried out contrast experiments between our work and the pure-uniform sampling methods [9, 10, 12] with the sampling parameters shown in Table 3.

Table 3. Sampling Parameters

Parameter Name	Uniform Sampling	Hybrid Sampling
Resolution of Terrain	32km×32km	32km×32km
Sampling step in pitch angle	0.02985(rad)	0.02985(rad)
Sampling step in azimuth angle	2π/80	0.09966~0.05807(rad)
Number of samplings in azimuth angle	80	80
Number of samplings in azimuth angle	105	47
Initial pitch angle	π/6	π/6

Three-dimensional visualization performances of radar coverage by our method in different environments are shown in Fig. 12 and Fig. 13.

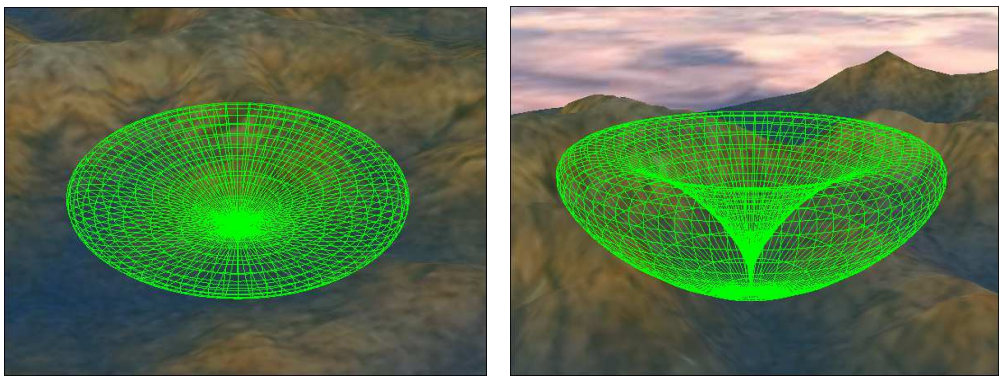

Fig. 12 3D visualization of radar coverage in free space

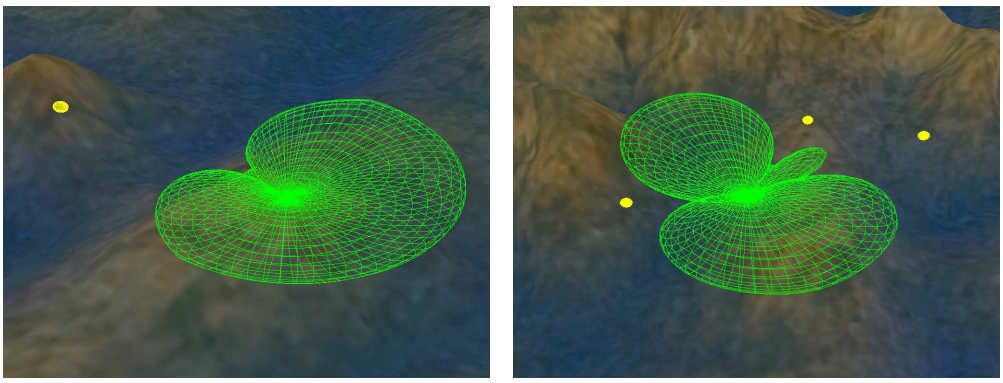

(a) Single source interference (b) Multi-source interference

Fig. 13 3D visualization of radar coverage under the influence of electromagnetic interference

To testify the performance of our method, firstly, we construct a scene, fix the viewpoint and estimate the maximum modeling capabilities of the methods above-mentioned. Experimental result is shown in Fig. 14.

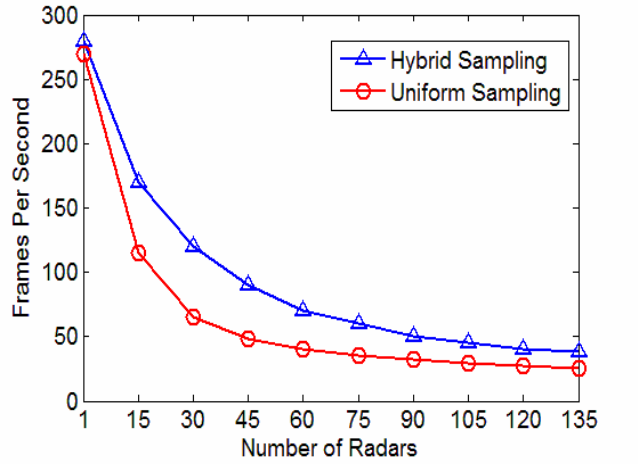

Fig. 14 Pressure test of uniform and hybrid sampling s in free space

Obviously, our method is more effective than uniform sampling approach. When the number of radars is up to 105, hybrid sampling still has 50 frames per second.

We also carried out a series of pressure tests on these two methods with radars scanning along pitch angle and horizontal movement in free space. The results are shown in Fig. 15 and Fig. 16.

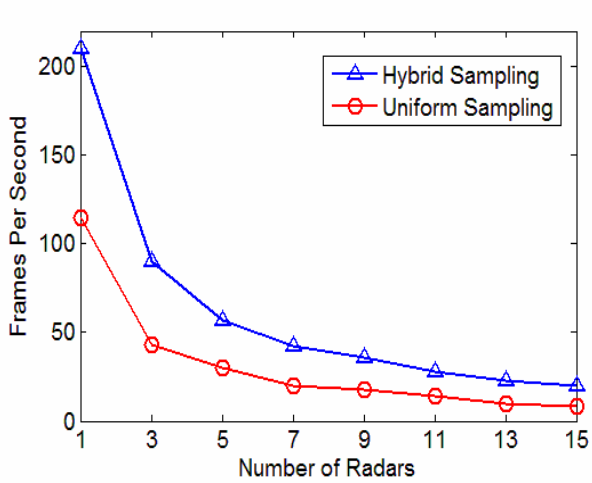

Fig. 15 Comparison of the frame rates when radars are in pitch scanning

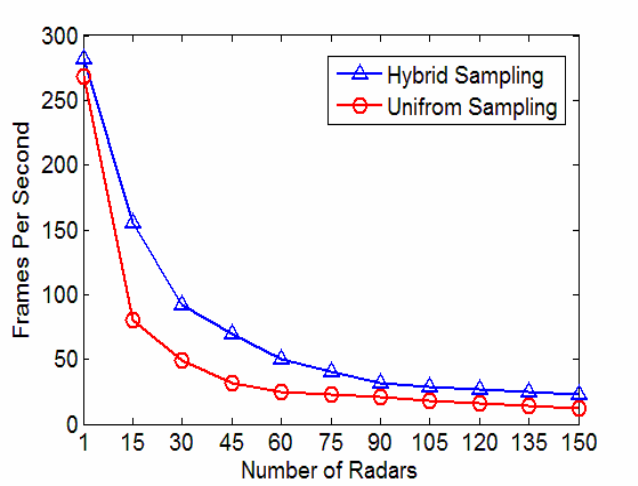

Fig. 16 Comparison of the frame rates when radars in movement

To testify the efficiency of our LOD-based acceleration strategy, firstly, we applied the parameters shown in Table 4 to construct the full resolution model of radar.

Table 4. Parameters list

Parameter Name	Values
Resolution of terrain	4000kw
Sampling step in pitch angle	3000MHz
Sampling step in azimuth angle	40dB
Number of sampling in azimuth angle	-10dBi
Number of sampling in pitch angle	250HZ
Initial pitch angle	12dB

Table 5 depicts the number of sampling points of different levels of detail.

Table 5. Number of sampling points

Level	Number of sampling points
$l=0$	34320
$l=1$	16008
$l=2$	8004
$l=3$	4002
$l=4$	2070

We rendered 10 radars in a scene. All the radars are in stationary state, and the fly-through path is predefined. We did two groups of experiments with and without LOD acceleration strategy. We sampled 5000 frames in each scene respectively, and achieved the average frame rate. The results are shown in Table 6.

Table 6. Average rendering speed with/without LOD

LOD State	Average rendering speed
on	73.9 fps
off	41.4 fps

6 Conclusion

Visualization of electromagnetic information is a research hotspot in the field of scientific computation visualization. This paper presents a method for three-dimensional visualization of radar coverage considering the electromagnetic interference, which ensures invariability of radar's feature and shape while greatly cuts the computing expense. It is more practical in real time applications that reflect radar coverage.

Acknowledgement:
The authors wish to thank the anonymous reviewers for their thorough review and highly appreciate the comments and suggestions, which significantly contributed to improving the quality of this paper.

This work is supported by National High Technology Research and Development Program of China (No. 2012AA011503), Project on the Integration of Industry, Education and Research of Guangdong Province (No. 2012B090600008) and the pre-research project (No. 51306050102).

References:

[1] Y. M. Lin, F. Zhang, W. Hu, A novel 3D visualization method of SAR data, *In Proc. Radar2013*, Xi'an, China, 2013, pp. 1-4.

[2] D. Fernando, N. D. Kodikara, C. Keppitiyagama, 3D radar – modeling virtual maritime environment for the static environment perception, *In Proc. ROBINONETICS '13*, Yogyakarta, Indonesia, 2013, pp. 176-181

[3] Q. S. Mahdi, Modeling of 3D pencil beam radar (PBR) volume coverage and 3D DMC, *In Proc. LAPC'10*, Loughborough, UK, 2010, pp. 621-624.

[4] L. S. Yang, J. Xu, X. Gao, et al, A novel three-dimensional coverage visualization system of netted radars based on ArcObjects, *In Proc. Radar'09*, Guilin, China, 2009, pp. 1-5.

[5] W. Zhang, B. L. Chen, S. H. Jin, The visual technology of the detection range in search radar, *Modern Radar*, No.3, 2000, pp. 44-47. (in Chinese)

[6] W. M. Lin, D. Q. De, Three-dimensional display of radar survey scope using OpenGL technique, *Journal of Wuhan University of Technology*, Vol.26, No.1, 2002, pp. 72-75. (in Chinese)

[7] A. Kostic, D. Rancic, Radar coverage analysis in virtual GIS environment, *In Proc.*

TELSIKS'03, Nis, Yugoslavia, 2003, pp. 721-724.

[8] D. Rancic, A. Dimitrijevic, A. Milosavljevic, et al, Virtual GIS for prediction and visualization of radar coverage, *In Proc. VIIP'03*, Benalmadena, Spain, 2003, pp. 970-974.

[9] G. M. Meng, Research on the representation technology of the radar detection range in the virtual battlefield environment, *Master dissertation*, National University of Defense Technology, China, 2005. (in Chinese)

[10] P. Chen, L. D. Wu, C. Yang, Research on representation of radar coverage in virtual battlefield environment considering terrain effect, *Journal of System Simulation*, Vol.19, No.7, 2007, pp. 1500-1503. (in Chinese)

[11] Y. Gao, W. Y. Liu, L. Lei, et al. Resarch on visualization of radar beam considering virtual environment effect, *In Proc. ITCS'10*, Kiev, Ukraine, 2010, pp. 353-356.

[12] F. M. Yang, G. Wan, F. Li, Research on 3D visualization of complicated battlefield electromagnetic environment, *Engineering of Surveying and Mapping*, Vol.21, No.2, 2012, pp. 35-38. (in Chinese)

[13] F. Li, Z. P. Zhang, G. Wang, et al, The 3D visualization technology of battlefield electromagnetic situation, *Journal of Geomatics Science and Technology*, Vol.29, No.3, 2012, pp. 222-225. (in Chinese)

[14] R. Awadallah, J. Z. Gehamn, J. R. Kuttler, et al, Modeling radar propagation in three-dimensional environments, *Johns Hopkins APL Technical Digest*, Vol.25, No.2, 2004, pp. 101-111.

[15] C. Yang, P. Chen, Y. M. Wei, Research and implementation of 3D visualization of radar maximum detection range, *Computer Engineering and Application*, Vol.43, No.11, 2007, pp. 245-248. (in Chinese)

[16] L. D. Wu, P. Chen, C. Yang, 3D representation of radar coverage in complicated environment, *System Engineering and Electronics*, Vol.30, No.8, 2008, pp. 1448-1453. (in Chinese)

[17] C. Peng, L. D. Wu, 3D representation of radar coverage in complex environment, *International Journal of Computer Science and Network Security*, Vol.7, No.7, 2007, pp. 139-145.

[18] P. Chen, Y. M. Wei, L. D. Wu, et al, Research and implementation of the 3D radar coverage visualization accelerated by hardware, *Computer Engineering & Science*, Vol.30, No.4, 2008, pp. 33-36. (in Chinese)

[19] J. Z. Zhang, X. J. Yuan, X. J. Zhao, et al, 3D visualization of radar detection range based on advanced propagation model, *Computer Engineering*, Vol.38, No.4, 2012, pp. 281-283. (in Chinese)